

CrossMark
click for updatesCite this: *RSC Adv.*, 2016, 6, 102336

Fe-assisted Ru clusters supported on porous and graphitic carbon for ammonia decomposition to CO_x free hydrogen†

L. Li,^{*a} F. Chen,^b Y. Dai,^a J. Wu,^a J. L. Shao^a and H. Y. Li^a

Porous and graphitic carbon supported Fe-assisted Ru cluster catalysts were prepared by a simple method. The textural and structural properties of the as-synthesized catalyst (Fe–C), the nearly pure carbon supported Ru catalyst (Ru/C[#]) and the Fe-assisted Ru catalyst (Ru/Fe–C) were characterized by X-ray diffraction, high transmission electron microscopy, Raman spectra, X-ray photoelectron spectroscopy, inductively coupled plasma-atomic emission spectrometer and N₂ sorption techniques. The analysis results revealed a micro/mesoporous carbon system with high surface area, uniform pore-size distribution and high graphitization degree. The Fe-assisted Ru clusters catalysts showed significantly improved performance for NH₃ decomposition compared to that of Fe–C and Ru/C[#] catalysts. It was concluded that Fe species not only played as a graphitization catalysts, but also promoted Ru catalysis, generating a synergistic effects during catalytic process.

Received 23rd August 2016
Accepted 18th October 2016

DOI: 10.1039/c6ra21211e

www.rsc.org/advances

1. Introduction

With the development of proton-exchange membrane fuel cells (PEMFC), the on-site generation of hydrogen has become an interesting alternative. In comparison to other carbonaceous H₂ precursors such as methane or methanol, NH₃ offers a higher H₂ storage capacity (17.7 wt%) and a higher energy density (3000 W h kg⁻¹). In addition, it can be easily stored and transported under mild conditions compared with hydrogen. And hydrogen source without CO_x are generated through catalytic decomposition of ammonia, which can be directly applied for fuel cell.^{1–4}

In the past decade, many different catalysts have been developed for ammonia decomposition. Many efforts have been devoted on the study of Ru,^{5–9} Ni,^{10–13} Fe^{14–17} based catalysts for ammonia decomposition. It has been demonstrated that Ru catalysts showed the highest catalytic activity among the common metal catalysts. Consequently, Ru-based catalysts have attracted particular attention for hydrogen production from ammonia because of their excellent catalytic performance.

Experimental observations have revealed that ammonia decomposition is a structurally sensitive reaction on the surface of Ru particles, and there is a close relationship between catalyst particle size and activity.^{6,18,19} Karim *et al.*⁶ conducted an

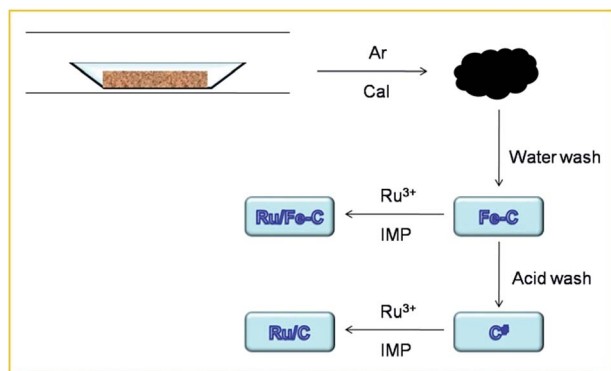
experimental and theoretical study and determined that the catalytic activity of Ru was dependent not only on the Ru particle size, but also on the Ru particle shape. Moreover, the catalytic performance of catalyst is also influenced significantly with various supports. Yin *et al.*¹⁹ found that carbon nanotubes (CNTs) supported Ru catalyst showed the highest catalytic performance, which is mainly related to the high Ru dispersion on CNTs, and to the high graphitization and high purity of CNT materials. Li and coworkers²⁰ further demonstrated that the higher graphitic degree of carbon used as supports showed better catalytic performance. Combining Ru nanoparticles with two-dimensional graphene nanosheets that forms a novel composite catalyst showed excellent ammonia decomposition activity.²⁶ Meanwhile, the interaction between Ru particles and the corresponding support, as well as the presence of the remaining surface functional groups on the support, can also influence the electronic structure of Ru atoms, which is vital to the reactivity of the corresponding Ru particles as well.^{21,22} Through these studies, it is well-accepted that the activity is closely related to the nature and structure of the carbon materials supports.

In the present study, we report a facile method used to prepare porous and graphitic carbon supported Ru-based catalyst for ammonia decomposition (Scheme 1). During the preparation process, the soluble NaCl was used as a porous structure-directing template, and Fe species were employed as carbon graphitization catalyst. We further compared the activity of three different catalysts: Fe–C, Ru/C[#] and Ru/Fe–C catalysts. The Ru/Fe–C catalyst showed the best catalytic activity among these catalysts. The results from the present study show that

^aSchool of Chemistry and Chemical Engineering, Yancheng Institute of Technology, Yancheng 224051, China. E-mail: lee_ycit@yahoo.com

^bSchool of Chemical Biology and Materials Engineering, Suzhou University of Science and Technology, Jiangsu, 215009, China

† Electronic supplementary information (ESI) available. See DOI: 10.1039/c6ra21211e



Scheme 1 Illustration of preparation process for the Fe-C, Ru/Fe-C and Ru/C[#] catalysts, respectively.

this novel composite can be used as an efficient and promising catalyst for ammonia decomposition or synthesis.

2. Experimental section

Catalyst preparation

The synthesis procedure for several compared catalysts were shown in Scheme 1 according to reported method.²³ Typically, carbon precursor C₆H₁₂O₆ (0.1 mol), metal precursor Fe(NO₃)₃·9H₂O (2 mmol), and soluble-template sodium chloride (8.766 g) were sequentially dissolved in deionized water. The resulting mixed solution was dried in drying oven and then ground by agate mortar to obtain fine composite powders. For the carbonization, the composite powders were heated at 850 °C for 2 h in a tube furnace under Ar (50 ml min⁻¹). Once cooled to room temperature, the obtained powder was first treated with deionized water to dissolve sodium chloride, and the treated sample was denoted as Fe-C catalyst. The Ru/Fe-C sample was obtained by wetness incipient impregnation method using the Fe-C sample and RuCl₃·xH₂O precursor with acetone as solvent, followed by drying at 328 K for 5 h and calcination at 823 K for 2 h in Ar flow. The nearly pure porous carbon materials (named C[#]) were obtained by treating Fe-C sample with hydrochloric acid to eliminate Fe-oxidic nanoparticles. The Fe-C sample was dispersed in 50 wt% HCl solution and refluxed at 90 °C for 6 h. And the Ru/C[#] sample was obtained by wetness incipient impregnation method using the pure carbon materials and RuCl₃·xH₂O precursor with acetone as solvent, followed by drying at 328 K for 5 h and calcination at 823 K for 2 h in Ar flow.

Catalyst characterization

N₂ adsorption analysis was performed at 77 K using a Micromeritics ASAP 2020 to access the surface areas and pore size distributions. All the samples were outgassed at 200 °C for 12 h. Then adsorption-desorption processes were conducted between the relative pressure (P/P_0) range from 10⁻⁶ to 1. The specific surface area was calculated by the conventional Brunauer-Emmette-Teller (BET) method. The pore size

distribution (PSD) plot was recorded by the DFT model. The micropore volume (V_{micro}) was estimated by using the t -plot method.

Powder X-ray diffraction (XRD) patterns were recorded on a Philips X'Pert MPD Pro X-ray diffractometer with graphite-monochromatized Cu K α radiation at a scanning rate of 2° per min in the 2θ range from 10° to 80°.

The morphology and microstructure of the HPC materials were studied by a FEI Tecnai G2 F20 transmission electron microscope (TEM) using an accelerating voltage of 200 kV.

X-ray photoelectron spectroscopy (XPS) analyses were carried out using a JPS-90MS photoelectron spectrometer (JEOL, Japan) with Mg K α radiation ($h\nu = 1253.6$ eV) in a vacuum of <10⁻⁷ Pa. The C-C peak position was set to 284.8 eV and taken as an internal standard.

The Inductively Coupled Plasma-Atomic Emission Spectrometer (ICP-AES) with a type of ELAN 9000 was used to determine the Ru contents.

Raman spectra were collected from 200 to 2000 cm⁻¹ on a Renishaw 2000 Confocal Raman Microprobe (Renishaw Instruments, England) using a 514.5 nm argon ion laser.

Catalytic activity

The activities of the catalysts were evaluated in a continuous flow quartz reactor with pure NH₃ (99.999%) feed at atmospheric pressure. The amounts of N₂ and unconverted NH₃ in the effluent were analyzed at room temperature by an online gas chromatography equipped with a thermal conductive detector (TCD) and a 3 m Poropak Q packed column and using H₂ as carrier gas. Blank tests indicated that the ammonia conversion in a blank reactor or over the supports was less than 1.0% at 600 °C.

3. Results and discussion

XRD patterns of graphitized carbon and their supported catalysts are presented in Fig. 1. It can be seen that all patterns exhibit two well-resolved diffraction peaks at about $2\theta = 26^\circ$ and

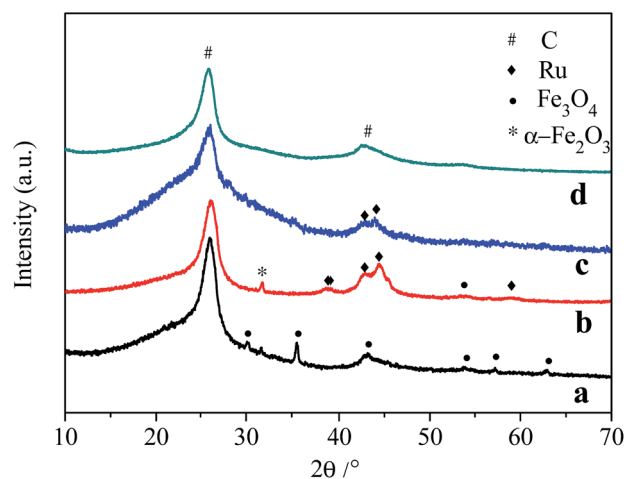


Fig. 1 XRD patterns of varied catalysts. (a) Fe-C (as synthesized), (b) Ru/Fe-C (after H₂ reduction), (c) Ru/C[#] (after H₂ reduction) and (d) C[#].

43°, which can be indexed as the (002) and (100) reflections of the graphitic carbon, respectively. After through water washing and HCl treatment, no NaCl and Fe phase were detected over carbon materials (C[#]) (Fig. 1d). As for Fe–C catalysts, only treated with water washing, show Fe₃O₄ crystallized phase. The peaks are located at 30°, 36°, 43°, 54°, 57° and 63°, corresponding to (100), (200), (310), (211), (301), (411) and (521) of Fe₃O₄ (JCPDS 01-089-2355), respectively. Subsequently, Ru clusters were introduced over carbon materials by a simple wet impregnation method. Contrast to Fe–C catalysts, it is found that Ru phase emerges after reducing in H₂ atmosphere. The diffraction peaks at about 2θ = 38°, 42°, 44° and 58° are assigned as the (100), (002), (101) and (102) reflections of Ru crystal phase (JCPDS 01-089-4903). In addition, the peak appearing in 2θ = 32° can be indexed to α-Fe₂O₃ (JCPDS 00-039-1346). Although all diffraction peaks are indexed, it is still difficult to distinguish the overlapping peaks at around 43°, which might be attributed to carbon, Ru and Fe₃O₄ species.

Fig. 2 shows (HR)TEM images of Ru/Fe–C and Ru/C[#] catalysts and their size distribution. Clearly, it is observed that carbon support exhibits foam like structures with a disordered

porosity. Ru clusters were homogeneously deposited onto the surface of graphitic carbon *via* a wet-impregnation method (Fig. 2A and C). And their particle size distributions in the composite are presented in Fig. 2B and D. For Ru/Fe–C catalyst, the size distribution of deposited Ru clusters is 2.21 ± 0.7 nm, except a few large particles. It might be speculated that Fe-oxidic species exist in the form of large particles by indirect correlation with the Ru/C[#] catalyst. Through the comparison of Fig. 2C, it was found that there were no large particles except smaller Ru clusters. During catalyst preparation procedure, the same procedure was adopted. It can be speculated that Fe-oxidic particles exhibit a large size. After treated with HCl solution, there remained large cave in carbon materials, also indirectly be related with pore volume of BET characterization. In addition, XRD and XPS characterization also verified the existence of Fe-oxidic particles. While the Ru/C[#] catalyst has an almost the same size distribution with a value of 2.25 ± 0.7 nm. Note that more Ru clusters over Ru/C[#] catalyst have a smaller size (<2 nm) compared with Ru/Fe–C catalyst. The nature of carbon support treated with HCl solution would further influence the particle size distribution of Ru clusters. Smaller Ru nanoparticles would provide more exposure of the active surface, which are readily accessible for guest molecules in catalysis. Previous studies also indicated that Ru crystallites with mean particle size of about 2.2 nm are extremely active for ammonia decomposition.²⁴ However, the over-dispersed catalyst may result in too small catalyst particles on the support, which may not provide enough space to accommodate the recombination of N atoms to form N₂ molecules.²⁵

HRTEM images (Fig. 2E and F) further provide detailed information about the structure of prepared catalysts. Fig. 2E demonstrates three different *d*-spacing patterns, 0.214, 0.234, and 0.341 nm, which are corresponding to Ru (002), Ru (100) and graphitic carbon species respectively. It is reported that the measured *d*-spacing of hexagonal Ru crystals with different crystallographic planes was 0.214, 0.205, 0.135, and 0.143 nm, which was consistent with the *d*-spacing values of (002), (101), (110), and (112) crystallographic planes of Ru crystals obtained by XRD.²⁶ The *d*-spacing value of Ru crystals can be assigned by the XRD diffraction. A *d*-spacing value of 0.341 nm can be indexed as (002) reflection of the graphitic carbon. As well-known that the graphitic carbon is mainly produced from the amorphous carbon which is in contact with the metal catalytic nanoparticles,²⁷ so the shape of all graphitic sheets exhibits cycle-like structure with different curvature. In addition, it also notes that lattice fringe of graphitic carbon exhibits discontinuous state, implying the prepared carbon is partly graphitized, which is also verified by Raman characterization.

N₂ sorption isothermals and pore size distributions of all porous carbon supported catalysts are illustrated in Fig. 3. All samples are typical of type-IV nitrogen sorption isothermals with H₄-type hysteresis loops, suggesting the existence of irregular pore structure. An obvious capillary condensation step at a medium relative pressure of (*P*/*P*₀) 0.45–0.95, implying a narrow mesopore diameter distribution. In addition, another N₂ sorption is observed at a relatively high pressure of 0.95–1.0, which can be attributed to the presence of macropores. The

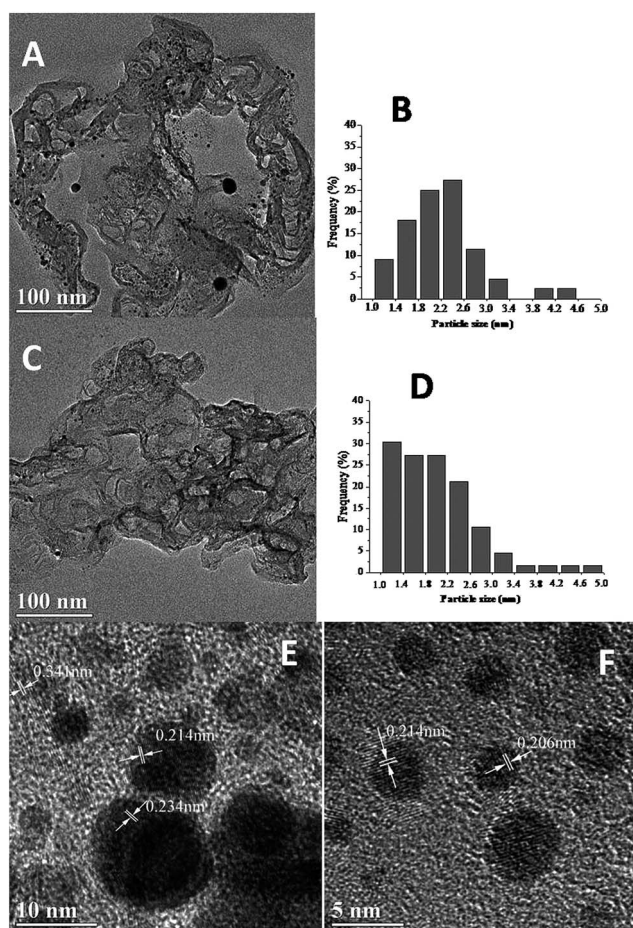


Fig. 2 (A, B and E) TEM images, the corresponding histograms of Ru particle size distribution and high-resolution TEM image of Ru/Fe–C catalysts. (C, D and F) TEM images, the corresponding histograms of Ru particle size distribution and high-resolution TEM image of Ru/C[#] catalysts.

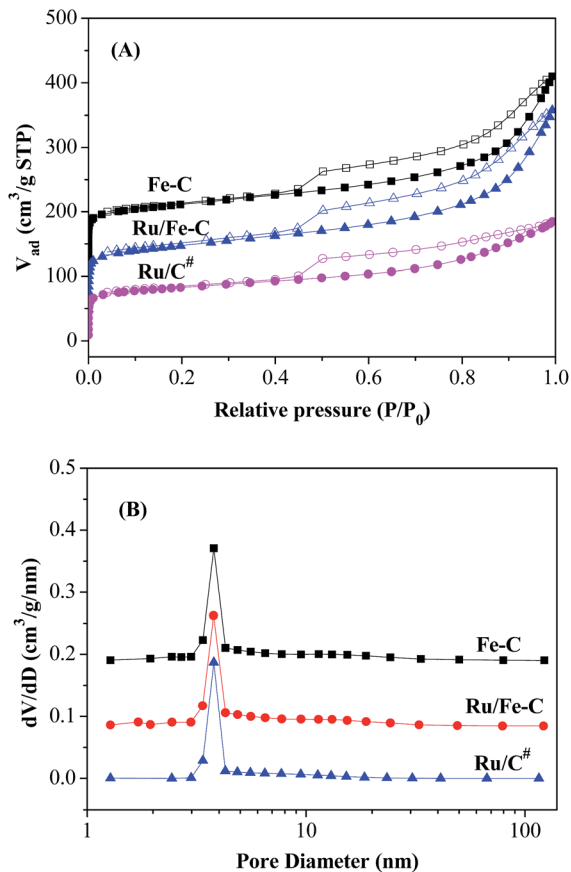


Fig. 3 (A) N_2 sorption isotherms and (B) pore-size distribution curves for different samples (Fe-C, Ru/Fe-C and Ru/C#).

calculated BET surface areas, pore volumes and pore sizes are shown in Table 1. It can be seen that the surface areas are range from 300 to $387 \text{ m}^2 \text{ g}^{-1}$ over different samples, and the corresponding total volumes vary from 0.258 to $0.402 \text{ cm}^3 \text{ g}^{-1}$. By means of micropore volumes data of different samples, it demonstrates that mesopore volume significantly reduces by removing Fe species from carbon materials.

Raman spectroscopy is an effective tool to study the properties of the different carbon materials, including crystalline, nanocrystalline and amorphous carbons. To further check the graphitic character, the pure carbon materials were characterized by Raman spectroscopy, as shown in Fig. 4. It is observed that two Raman bands center at ~ 1335 and $\sim 1580 \text{ cm}^{-1}$ respectively. The peak at 1580 cm^{-1} is the G band, characteristic feature of ordered graphite carbon, attributed to the vibration of sp^2 -bonded carbon atoms. Another peak at 1340 cm^{-1} is the D

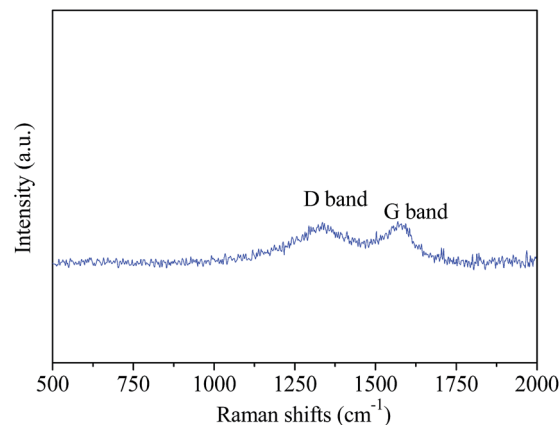


Fig. 4 Raman spectra of typical prepared carbon materials (C#).

band, associated with vibrations of carbon atoms with dangling bonds in plane terminations of the disordered graphite and related to the defects and disorders of structures in carbon materials.²⁰ The intensity ratios of the D-band to the G-band (I_D/I_G) (ratio of amorphous to graphitic carbon) was calculated to be 0.936 , indicating that the prepared carbon is partly graphitized. This is consistent with the above XRD and TEM analysis. In fact, the soluble NaCl was used as a porous structure-directing template, while Fe species were employed as graphitization catalyst during catalyst preparation process. Previous studies also demonstrated that porous graphitic carbons could be also prepared at relatively low temperature ($<1000 \text{ }^\circ\text{C}$) by means of heterogeneous graphitization, which was carried out with the aid of catalysts (*i.e.* Fe, Co, Ni, *etc.*).^{27,29–32}

The electronic state of the Ru, O and Fe elements in the catalyst were analyzed by XPS. Fig. 5a shows a survey of the XPS spectra of Ru/Fe-C and Ru/C# catalyst. Both samples show obvious peaks centered at the binding energies of around 533.1 and 287.4 eV , which are assigned to O 1s and C 1s XPS signals, respectively. Additional peaks centered at the binding energies of 484.08 and 461.08 eV are observed, which are assigned to Ru $3p_{1/2}$ and Ru $3p_{3/2}$ peaks, respectively. Weak Fe 2p peak is also observed at the binding energies of around 713.08 eV . Seen from Fig. 5b and c, in spite of the interference of the adventitious carbon, the XPS spectrum can be resolved fairly well with two spin-orbit-split doublets from two chemically different Ru entities and the C 1s peak. Although the catalysts were prepared from RuCl_3 precursor even by H_2 reduction at $500 \text{ }^\circ\text{C}$, it is difficult to remove chlorine. This is in agreement with the results of Mieth and Schwarz.³⁷ As shown in Fig. 5b and c,

Table 1 Physical properties of varied catalysts

Samples	Ru content ^a (wt%)	Fe content ^a (wt%)	Fe/Ru molar ratio	S_{BET} ($\text{m}^2 \text{ g}^{-1}$)	V_{micro} ($\text{cm}^3 \text{ g}^{-1}$)	V_{total} ($\text{cm}^3 \text{ g}^{-1}$)	D_p (nm)
Fe-C	—	1.16	—	366	0.086	0.378	4.12
Ru/Fe-C	0.97	1.15	2.14	387	0.093	0.402	4.15
Ru/C#	0.91	0.57	1.13	300	0.081	0.258	3.44

^a Determined by ICP-AES analysis.

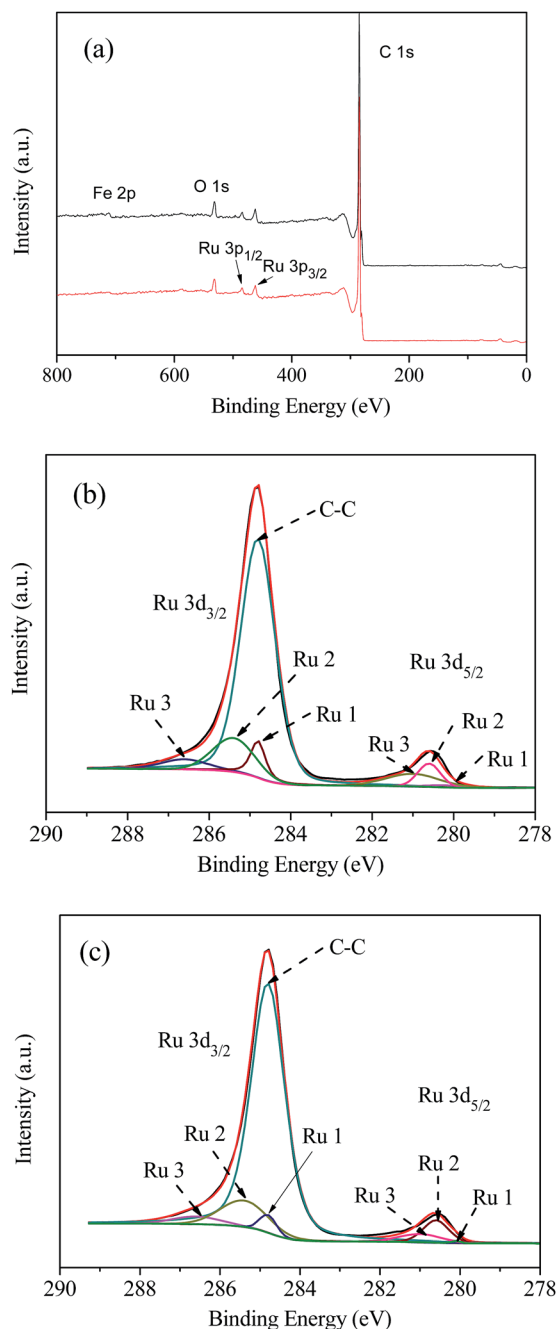


Fig. 5 (a) Survey XPS spectra of Ru/Fe-C and Ru/C[#] catalyst after reduction at 500 °C. (b) High-resolution Ru 3d XPS spectra of Ru/Fe-C. (c) High-resolution Ru 3d XPS spectra of Ru/C[#].

different Ru species were observed. A signal at 280.2 eV is attributed to Ru⁰, but not all Ru ions are reduced. The positions of the Ru 3d peak at 280.6 and 281.0 eV show the presence of RuO₂ and RuCl₃ species, respectively. As for the presence of Ru oxide, it is possible that Ru nanoparticles were passivated upon exposure to air.³³ Note that Ru⁰/Ru^{δ+} ratio in Ru/Fe-C catalyst is higher than that in Ru/C[#] catalyst as a comparison. Meanwhile, it is also observed that there is 0.3 eV difference over the electron binding energy of Ru 3p_{3/2} (Fig. S1†). In other words, the electron density of Ru on Ru/Fe-C is slight lower than that on Ru/C[#].

In order to further clarify the iron species over the surface of prepared catalyst, the Fe and O part of the spectra are measured and exploited. In Fig. S2,† the 2p Fe spectra are dominated by higher oxidation states (mainly Fe³⁺). And the number of Fe-oxidic species in Ru/Fe-C sample is obviously more than that in Ru/C[#] sample. While O 1s peaks at 531.95 eV and 530.7 eV are also attributed to the oxygen atoms in Fe₂O₃ and Fe₃O₄, respectively (Fig. S3†). These findings are consistent with above XRD results. Moreover, the peak integration of the 2p Fe and 3d Ru features are also illustrated in Table S1.† It can be seen that there exist almost identical Fe/Ru ratios over the surface composition of comparison samples. However, this is different from the Fe/Ru ratios over the bulk composition (Table 1). Note that the Ru/C[#] sample still has a Fe content of 0.57 wt%, though it was treated with 50 wt% HCl solution at 90 °C for 6 h. This means that the very little Fe-oxidic species embedded deeply in carbon matrix cannot be directly dissolved, which were also hard to be reduced by H₂. Similar finding was also verified by Lu *et al.*³⁹ The graphitic carbon-shell protected cobalt nanoparticles had been achieved *via* a pyrolysis process, which showed very high stability under strong acidic and basic conditions.

The catalytic activities of the prepared porous carbon supported Ru-based catalysts for NH₃ decomposition as a function of reaction temperature are presented in Fig. 6. Interestingly, it can be seen that there is basically no activity for Fe/C catalyst. It might be attributed to less iron species or unreduced Fe-oxidic species (Table 1). Once introducing Ru clusters into Fe-C samples, it shows better catalytic activity than the Ru/C[#] catalyst. It seems that the possible synergistic effect between Fe nanoparticles and Ru clusters appears to be beneficial for activity. In order to clarify the synergistic effects between Fe species and Ru on the surface of carbon support, XPS characterization was applied for study. In fact, the electron density of Ru on Ru/Fe-C is slight lower than that on Ru/C[#] catalyst, which do not contribute to the improvement of the catalytic activity. However, more Fe-oxidic species could be reduced by abundant generating H₂ at a high reaction temperature, forming Fe⁰ as single or dual active sites, which benefits to rising activity. On the other hand, the surface area and pore structure of the

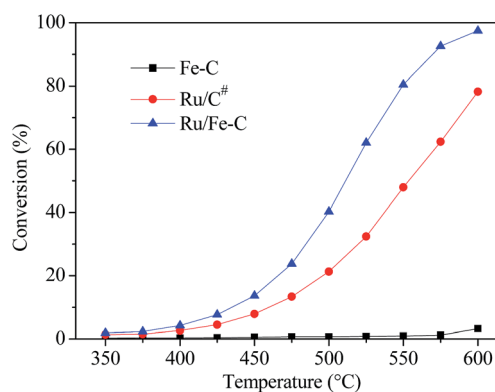


Fig. 6 Ammonia decomposition reaction activity test with Fe-C (■), Ru/Fe-C (▲) and Ru/C[#] (●) catalysts.

Table 2 Properties and activities of comparison catalysts

Samples	d_{Ru}^a (nm)	Dispersion ^b (%)	Conversion ^c (%)	H ₂ formation rate ^c (mmol min ⁻¹ g _{cat} ⁻¹)	TOF ^c (s ⁻¹)	E_a^d (kJ mol ⁻¹)
Ru/Fe-C	2.21	59.7	97.5	21.7	3.3	85.6
Ru/C [#]	2.25	58.7	78.2	17.4	2.7	91.4

^a Calculated on the basis of TEM images. ^b Calculated from the TEM results by employing the spherical model $D = 1.32/d$.^{8,28} ^c Obtained from the catalytic activities of Ru catalysts at 600 °C. GHSV = 20 000 ml h⁻¹ g_{cat}⁻¹. ^d Activation energy was measured under pure NH₃ flow at 375–450 °C.

catalyst may be another major factor in this reaction. The Ru catalysts supported on the Fe-doped carbons have a higher surface area than that supported on the pure carbons. Thus the Ru catalyst particles were well dispersed into the channel of the mesoporous carbon, which enhanced the adsorption of ammonia. Interestingly, although the Ru/Fe-C catalyst has a higher surface area and more mesopores, it still has a relative lower catalyst dispersion (larger Ru particle size) evidenced by TEM characterization. Previous studies indicated that a relatively larger catalyst particle can increase the catalytic activity.^{20,38} As mentioned in the beginning of this Section, N-H bond cleavage and recombinative desorption of surface nitrogen atoms instead of the NH₃ adsorption is the rate-limiting steps in ammonia decomposition. Over-dispersed catalyst may result in too small catalyst particles on the support, which may not provide enough space to accommodate the N-H split and the recombination of N atoms to form N₂ molecules.

In addition, there would be a correlation between the crystallites of the carbon support and activity, which was observed by Zhu's studies.²⁰ A lower graphitic degree results in the poor electron conductivity of the carbon support, thus resulting in the lower activity of the carbon supported catalyst. As mentioned before, both cleavage of N-H bond and recombinative desorption of surface nitrogen atoms may be the rate-limiting steps in ammonia decomposition on well-dispersed Ru catalyst.³⁴ Support or additive which can facilitate electron feedback to the antibonding orbital of the transient metal-nitrogen bond should be beneficial for these steps.³⁵ In terms of CNTs, it is a superior support for ammonia decomposition because of its high metal dispersion and good degree of graphitization, which is beneficial for the electron transfer between support and Ru.¹ In our studies, porous carbon support with a certain degree of graphitization is also benefit for improving catalytic performance of Ru-based catalyst.

For comparison, Table S2† summarizes the catalytic performance of Ru/Fe-C and other typical Ru-based catalysts reported previously for ammonia decomposition. No doubt that Ru supported by CNTs (Ru/CNTs) was considered to be a high-performance catalyst for ammonia decomposition. However, Ru loading over CNTs has an important effect on activity. 5 wt% Ru loading catalyst shows better catalytic performance than that with around 1 wt% Ru loading. Note that our prepared Ru/Fe-C catalyst showed a comparable activity with 1 wt% Ru/CNTs catalyst prepared by Chang *et al.*³⁶ Although the activity of Ru/Fe-C catalyst is lower than that of graphene or CTF supported Ru-based catalyst, the prepared process is relatively simple and

easy to large-scale production. Moreover, the durability of the Ru/Fe-C catalyst in ammonia decomposition was tested for the catalytic decomposition of ammonia at 550 °C for a period of 50 h. As shown in Fig. S4,† ammonia conversion is almost constant, indicating a very stable catalytic performance at high temperature.

In addition, the turnover frequency (TOF) of NH₃ and the apparent activation energies (E_a) are presented in Table 2. The turnover frequency (TOF) of NH₃ can be calculated from the amount of converted NH₃ molecules per exposed surface Ru atom in unit time.^{8,28} Specifically, the number of reacted molecules is obtained by the conversion and flow rate of ammonia at the corresponding temperature, while the number of the available surface Ru atoms of each catalyst is calculated from the dispersion of Ru atoms measured by TEM, as shown in Table 1. With the help of Fe assistance, the Ru/Fe-C catalyst exhibits a higher TOF value (3.3 s⁻¹) than that of Ru/C[#] catalyst (2.7 s⁻¹).

The apparent activation energies (E_a) were obtained from the Arrhenius relationship between the rate constant (k) and the temperature (T), which can be described by the equation: $\ln(k) = -E_a/RT + \text{constant}$, and the results are listed in Table 2. It can be seen that the activation energy of Ru/Fe-C catalyst obtained from the Arrhenius plots (Fig. 7) is 85.6 kJ mol⁻¹, which is lower than that of Ru/C catalyst (91.4 kJ mol⁻¹). It indicates that Fe additives are facilitate the molecular activation during reaction process. Moreover, the E_a values in our studies are similar to the reported E_a value of Ru/CNTs catalyst.³⁶

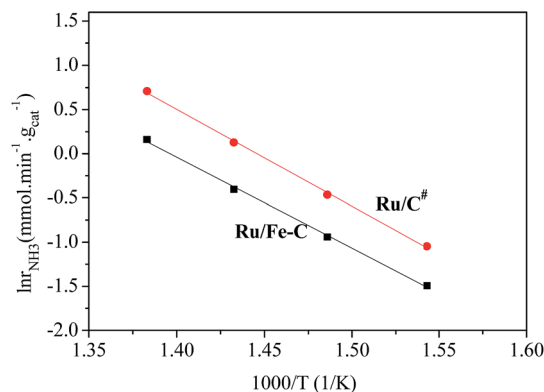


Fig. 7 Arrhenius plots of Ru/C[#] (●) and Ru/Fe-C catalyst (■). The temperature range (375–450 °C) used for the determination of apparent activation energies was based on NH₃ conversion values far away from the equilibrium values.

4. Conclusions

Porous and graphitic carbon supported Fe-assisted Ru cluster catalysts were prepared by a simple method. Characterization results revealed the prepared catalysts with high surface area, uniform pore-size distribution and high graphitization degree. Owing to Fe assistance, the Ru/Fe-C catalyst showed significantly improved performance for NH₃ decomposition compared to that of Fe-C and Ru/C[#] catalysts. The NH₃ conversion over the Ru/Fe-C catalyst is 97.5% (600 °C and 20 000 ml h⁻¹ g_{cat}⁻¹), and TOF_{NH₃} is 3.3 s⁻¹. The activation energy of Ru/Fe-C catalyst is 85.6 kJ mol⁻¹, which is lower than that of Ru/C[#] catalyst. It was concluded that Fe species not only played as a graphitization catalysts, but also promoted Ru catalysis, generating a synergistic effects during catalytic reaction process.

Acknowledgements

This work was supported by the National Natural Science Foundation of China (21503184, 21407111), Talent introduction project of Yancheng institute of technology (xj201507). And the research fund of Collaborative Innovation Center for Ecological Building.

References

- S. F. Yin, B. Q. Xu, X. P. Zhou and C. T. Au, *Appl. Catal.*, 2004, **277**, 1–9.
- R. Lan, J. T. S. Irvine and S. W. Tao, *Int. J. Hydrogen Energy*, 2012, **37**, 1482–1494.
- F. Schüth, R. Palkovits, R. Schlögl and D. S. Su, *Energy Environ. Sci.*, 2012, **5**, 6278–6289.
- E. García-Bordejé, S. Armenise and L. Roldán, *Catal. Rev.*, 2014, **56**, 220–237.
- S. F. Yin, Q. H. Zhang, B. Q. Xu, W. X. Zhu, C. F. Ng and C. T. Au, *J. Catal.*, 2004, **224**, 384–396.
- A. M. Karim, V. Prasad, G. Mpourmpakis, W. W. Lonergan, A. I. Frenkel, J. G. Chen and D. G. Vlachos, *J. Am. Chem. Soc.*, 2009, **131**, 12230–12239.
- W. Q. Zheng, J. Zhang, B. Zhu, R. Blume, Y. Zhang, K. Schlichte, R. Schlögl, F. Schüth and D. S. Su, *ChemSusChem*, 2010, **3**, 226–230.
- L. Li, Y. Wang, Z. P. Xu and Z. H. Zhu, *Appl. Catal.*, A, 2013, **467**, 246–252.
- A. K. Hill and L. Torrente-Murciano, *Appl. Catal.*, B, 2015, **172–173**, 129–135.
- J. Zhang, H. Xu, X. Jin, Q. Ge and W. Li, *Appl. Catal.*, A, 2005, **290**, 87–96.
- W. Zheng, J. Zhang, Q. Ge, H. Xu and W. Li, *Appl. Catal.*, B, 2008, **80**, 98–105.
- H. Muroyama, C. Saburi, T. Matsui and K. Eguchi, *Appl. Catal.*, A, 2012, **443–444**, 119–124.
- J. Ji, X. Duan, G. Qian, X. Zhou, D. Chen and W. K. Yuan, *Ind. Eng. Chem. Res.*, 2013, **52**, 1854–1858.
- Y. Li, S. Liu, L. Yao, W. Ji and C. T. Au, *Catal. Commun.*, 2010, **11**, 368–372.
- A. H. Lu, J. J. Nitz, M. Comotti, C. Weidenthaler, K. Schlichte, C. W. Lehmann, O. Terasaki and F. Schüth, *J. Am. Chem. Soc.*, 2010, **132**, 14152–14162.
- X. Z. Duan, G. Qian, X. Zhou, Z. Sui, D. Chen and W. K. Yuan, *Appl. Catal.*, B, 2011, **101**, 189–196.
- M. Feyen, C. Weidenthaler, R. Güttel, K. Schlichte, U. Holle, A. H. Lu and F. Schüth, *Chem.-Eur. J.*, 2011, **17**, 598–605.
- W. Zheng, J. Zhang, H. Xu and W. Li, *Catal. Lett.*, 2007, **119**, 311–318.
- S. F. Yin, B. Xu, W. Zhu, C. Ng, X. Zhou and C. T. Au, *Catal. Today*, 2004, **93**, 27–38.
- L. Li, Z. H. Zhu, Z. F. Yan, G. Q. Lu and L. Rintoul, *Appl. Catal.*, A, 2007, **320**, 166–172.
- F. R. Garcia-Garcia, J. Alvarez-Rodriguez, I. Rodriguez-Ramos and A. Guerrero-Ruiz, *Carbon*, 2010, **48**, 267–276.
- J. Chen, Z. H. Zhu, Q. Ma, L. Li, V. Rudolph and G. Q. Lu, *Catal. Today*, 2009, **148**, 97–102.
- N. Q. Zhao, S. Wu, C. N. He, C. S. Shi, E. Z. Liu, X. W. Du and J. J. Li, *Mater. Lett.*, 2012, **87**, 77–79.
- J. Zhang, H. Y. Xu, Q. J. Ge and W. Z. Li, *Catal. Commun.*, 2006, **7**, 148–152.
- C. J. H. Jacobsen, S. Dahl, P. L. Hansen, E. Törnqvist, L. Jensen, H. Topsøe, D. V. Prip, P. B. Møenshaug and I. Chorkendorff, *J. Mol. Catal. A: Chem.*, 2000, **163**, 19–26.
- G. Li, H. Nagasawa, M. Kanezashi, T. Yoshiok and T. Tsuru, *J. Mater. Chem. A*, 2014, **2**, 9185–9192.
- D. W. Wang, F. Li, M. Liu, G. Q. Lu and H. M. Cheng, *Angew. Chem., Int. Ed.*, 2008, **47**, 373–376.
- L. Wang, J. L. Chen, L. Ge, Z. H. Zhu and V. Rudolph, *Energy Fuels*, 2011, **25**, 3408–3416.
- M. Sevilla and A. B. Fuertes, *Carbon*, 2006, **44**, 468–474.
- D. Y. Zhai, H. D. Du, B. H. Li, Y. Zhu and F. Y. Kang, *Carbon*, 2011, **49**, 725–729.
- W. J. Gao, Y. Wan, Y. Q. Dou and D. Y. Zhao, *Adv. Energy Mater.*, 2011, **1**, 115–123.
- Y. P. Zhai, Y. Q. Dou, X. X. Liu, S. S. Park, C. S. Ha and D. Y. Zhao, *Carbon*, 2011, **49**, 545–555.
- H. B. Dai, X. Kang and P. Wang, *Int. J. Hydrogen Energy*, 2010, **35**, 10317–10323.
- M. C. J. Bradford, P. E. Fanning and M. A. Vannice, *J. Catal.*, 1997, **172**, 479–484.
- F. Hayashi, Y. Toda, Y. Kanie, M. Kitano, Y. Inoue, T. Yokoyama, M. Hara and H. Hosono, *Chem. Sci.*, 2013, **4**, 3124–3130.
- F. Chang, J. P. Guo, G. T. Wu, L. Liu, M. Zhang, T. He, P. K. Wang, P. Yu and P. Chen, *RSC Adv.*, 2015, **5**, 3605–3610.
- J. Mieth and J. Schwarz, *J. Catal.*, 1989, **118**, 218–226.
- S. G. Chen and R. T. Yang, *J. Catal.*, 1993, **141**, 102–113.
- A. H. Lu, W. C. Li, N. Matoussevitch, B. Spliethoff, H. Bönemann and F. Schüth, *Chem. Commun.*, 2005, 98–100.